

# It’s always the quiet ones: Single Degenerate Double Detonation Type Ia Supernova from Quiescent Helium Accretion

AMIR MICHAELIS <sup>1</sup>, YAEL HILLMAN <sup>2,1</sup> AND HAGAI B. PERETS <sup>1,3</sup>

<sup>1</sup>*Department of Physics Technion — Israel Institute of Technology Haifa 3200003, Israel*

<sup>2</sup>*Department of Physics, Azrieli College of Engineering, Ramat Beit Hakerem, POB 3566, Jerusalem 91035, Israel*

<sup>3</sup>*Astrophysics Research Center of the Open University (ARCO), The Open University of Israel, P.O Box 808, Ra’anana 4353701, Israel*

## ABSTRACT

We investigate a sub-Chandrasekhar mass double detonation pathway for Type Ia supernovae arising from single degenerate helium accreting carbon-oxygen white dwarfs. Building on our previous one dimensional study of recurrent helium novae (Hillman et al. 2025), we evolve a  $0.7 M_{\odot}$  white dwarf through steady accretion at  $10^{-8} M_{\odot} \text{ yr}^{-1}$  until it reaches  $1.1 M_{\odot}$ , yielding realistic, time evolved helium rich profiles. These profiles are mapped into FLASH simulations, incorporating nuclear burning for helium and carbon–oxygen detonation, in multi-dimensional hydrodynamic runs. A localized, modest temperature perturbation near the base of the helium shell robustly triggers an outward helium-shell detonation. The ensuing inward propagating shock converges in the carbon–oxygen core, igniting a secondary detonation that unbinds the star. We obtain a  $^{56}\text{Ni}$  yield of  $\simeq 0.64 M_{\odot}$ , an intermediate-mass element (Si-Ca) mass of  $\simeq 0.41 M_{\odot}$ , and maximum ejecta velocities approaching  $\sim 22,000 \text{ km s}^{-1}$  - values consistent with normal Type Ia supernovae. Our results demonstrate that recurrent helium accretors—typically quiescent over long timescales—can evolve under subtle, “quiet” conditions to trigger robust double detonations, supporting their role as viable progenitors of sub-Chandrasekhar mass Type Ia supernovae.

## 1. INTRODUCTION

Type Ia supernovae (SNe Ia) are indispensable tools for cosmology (Brout et al. 2019; Galbany et al. 2023; Palicio et al. 2024) and major contributors to galactic iron-peak enrichment (Tang & Wang 2010; De et al. 2014; Cavichia et al. 2024; Bhattacharya et al. 2025), yet decades of study have not yielded a consensus on their progenitors (Howell 2011; Maoz et al. 2014; Hoefflich 2017; Jha et al. 2019; Liu et al. 2023; Soker 2024, 2025a; Ruiter & Seitzzahl 2025). Classical single-degenerate (SD) models (Whelan & Iben 1973; Nomoto 1982a) invoke a carbon–oxygen white dwarf (CO WD) ac-

creting from a non-degenerate companion until reaching the Chandrasekhar mass ( $\sim 1.4 M_{\odot}$ ), where ignition proceeds via a deflagration-to-detonation transition (Khokhlov 1991; Plewa et al. 2004; Gamezo et al. 2004, 2005) or a gravitationally confined detonation in multi-dimensional simulations (Calder et al. 2004; Meakin et al. 2009; Jordan et al. 2008, 2012). However, deep late-time nebular spectra of nearby SNe Ia (e.g., SN 2011fe) show no H $\alpha$  or He I emission down to  $\lesssim 10^{-4} M_{\odot}$  of stripped companion material, and pre-explosion imaging together with early-time UV limits rule out a bright red-giant, placing stringent constraints

on classic SD channels (Li et al. 2011; Nugent et al. 2011). Observations of SN 2022xkq and SN 2023bee—showing fast declines and/or early flux excesses—pose additional challenges to current progenitor and explosion models (Pearson et al. 2024; Wang et al. 2024).

An alternative double-degenerate (DD) pathway involves the merger of two WDs via gravitational-wave-driven inspiral. If the combined mass exceeds  $\sim 1.4 M_{\odot}$ , central carbon ignition may occur (“classical” DD; Webbink 1984; Iben & Tutukov 1984), but off-center burning can instead form an O–Ne WD rather than a supernova (Saio & Nomoto 1998; Shen et al. 2012). More recently, “dynamically driven double-degenerate double detonations” ( $D^6$ ; Shen et al. 2010; Pakmor et al. 2013; Boos et al. 2024; Pollin et al. 2025) and head-on collisions (Raskin et al. 2009; Kushnir et al. 2013; Glanz et al. 2025) have been shown to produce prompt, sub-Chandrasekhar detonations in one or both WDs. Both SD and DD channels predict delay-time distributions (DTD)  $\propto t^{-1}$  over 0.1–10 Gyr (Friedmann & Maoz 2018; Freundlich & Maoz 2021), consistent with observed SN Ia rates in old stellar populations, yet neither channel cleanly satisfies all spectroscopic and rate constraints.

Recent work has also highlighted the role of hybrid CO–He white dwarfs in the DD landscape. In these systems, one or both WDs possess a CO core surrounded by a thick helium mantle. During the merger, the less massive hybrid can tidally disrupt and deposit a substantial He layer onto the primary, creating conditions for an edge-lit detonation at sub-Chandrasekhar mass (Perets et al. 2019; Pakmor et al. 2021). Population-synthesis studies suggest that hybrid (He–CO) WDs are common in close binaries and that a large fraction of double-WD mergers involve at least one hybrid. In some models, CO+hybrid mergers contribute at levels comparable to CO+CO merg-

ers to the overall SN Ia rate and DTD, though assumptions about common-envelope efficiency and metallicity can shift the balance (Nelemans et al. 2001; Toonen et al. 2017; Liu et al. 2017).

In parallel, Soker (2025a) has proposed a double-degenerate merger-to-explosion-delay (DD-MED) scenario, in which two CO WDs merge and explode after a  $\sim 1$ –2 yr relaxation phase, potentially explaining SN Ia interactions with CO-rich circumstellar material at  $\gtrsim 50$  days post-explosion. This delayed detonation within a merger remnant again highlights that “quiet,” non-traditional channels may hide within the SN Ia population.

Against this backdrop, the sub-Chandrasekhar “double-detonation” scenario has emerged as a robust alternative: a CO WD accretes a thin He shell that detonates first, sending a shock into the core that triggers a secondary carbon–oxygen detonation (Nomoto 1982b). Multi-dimensional studies demonstrate that even shells as low as  $\sim 0.03 M_{\odot}$  can focus a strong inward shock and robustly detonate the core—yielding normal-luminosity SNe Ia without fine tuning (Pakmor et al. 2022). Synthetic light curves predict early UV/optical “bumps” from shell ashes, and high-velocity Ca II/Ti II absorption features in the first days—features that are now being sought in high-cadence surveys (Yao et al. 2019; Piro & Nakar 2025).

A critical uncertainty in these models has been the physical origin and composition of the He shell. One scenario that in certain cases may allow for a helium shell to gradually accumulate on the surface of a WD, is as the product of nova eruptions. In this case, the system would be a cataclysmic variable (CV) where mass is transferred through the inner Lagrangian point (L1) (Shara 1981; Prialnik & Kovetz 1995; Yaron et al. 2005; Shara et al. 2018; Hachisu & Kato 2010), or a symbiotic system, for which the wind from a red giant (RG) or an asymptotic giant branch star (AGB) is either gravitation-

ally captured by the WD via the Bondi-Hoyle-Littleton (BHL) mechanism, (Mikolajewska & Kenyon 1992; Mikolajewska 2008, 2010; Hillman & Kashi 2021; Vathachira et al. 2024, 2025a) or if the binary orbit is close enough, via wind focusing through L1, i.e., wind Roche-lobe overflow (WRLOF) (Abate et al. 2013; Saladino et al. 2019; Vathachira et al. 2025b). Regardless of the mass transfer mechanism, the result is hydrogen-rich material being accumulated on the surface of the degenerate WD, which eventually ignites in a runaway process and produces a nova eruption (e.g., Gallagher & Starrfield 1978; Starrfield & Sparks 1987; Warner 1995). Models have shown that if the hydrogen (H) is accreted at a high enough rate, the eruption will not eject all the mass that has been accreted, but will leave behind a He-rich residue (Kato & Hachisu 1999, 2004; Hillman et al. 2016). This helium may accumulate over many H-novae, until eventually reaching its own critical mass that triggers a He-nova (José et al. 1993; Idan et al. 2013; Newsham et al. 2014). Based on this, we Hillman et al. (2015) followed the results of the one-dimensional nova-simulation code accreting hydrogen at a high rate, and used the average accumulation rate of He-rich material as the input for direct helium accretion. Our results showed periodic helium novae that, after a long adaptation period, became less degenerate and led to the growth of the CO core.

Acknowledging that helium could accumulate on the surface of a WD via the by-product of nova eruptions, or via direct accumulation from a He-star (or a He-WD), leading to a wide possibility of accumulation rates, Hillman et al. (2025) followed helium-accretion on CO WDs ( $0.65\text{--}1.0 M_{\odot}$ ) at different rates  $\dot{M} \sim 10^{-5} - 10^{-10} M_{\odot} \text{ yr}^{-1}$ , showing that while the high rates produce recurrent novae, for the regime  $\lesssim 10^{-8} M_{\odot} \text{ yr}^{-1}$  helium need not ignite promptly; the system may avoid nova eruptions and continue to accrete helium until a

thermonuclear runaway (potentially a SN Ia or an undetermined transient, UT). These models produce helium shells of order a few  $\times 10^{-2} M_{\odot}$  up to a few  $\times 10^{-1} M_{\odot}$  that naturally accumulate before runaway at sub-Chandrasekhar masses. These time-evolved profiles—complete with realistic thermal and compositional gradients—offer physically motivated initial conditions for multi-dimensional detonation simulations, in contrast to ad hoc shell prescriptions.

Here, we unite detailed He-nova evolution with multi-dimensional hydrodynamics by mapping an initial  $0.7 M_{\odot}$  WD that quiescently accretes He-rich material at a rate of  $\dot{M} = 10^{-8} M_{\odot} \text{ yr}^{-1}$  until reaching  $1.1 M_{\odot}$ . We entered the WD profile into FLASH simulations (Fryxell et al. 2000), incorporating 19-element nuclear burning for both helium and carbon–oxygen. By seeding a modest temperature perturbation at a random point on the shell–core interface, we capture the double-detonation mechanism—the outward He-shell detonation, inward shock convergence, and subsequent core detonation. We then quantify explosion energetics, nucleosynthesis yields, and ejecta kinematics, providing a unified, physically motivated demonstration that quiescent helium accretors can robustly produce normal-luminosity SNe Ia in a double-detonation single-degenerate scenario. Section 2 describes our 1D and FLASH setups; Section 3 presents our results; Section 4 discusses implications for progenitor demographics and observations; and Section 5 summarizes our conclusions.

### 1.1. *Double-detonations with thick vs. thin helium shells*

Early sub-Chandrasekhar studies showed that detonating a sufficiently massive helium (He) shell can drive a converging shock into the C/O core and ignite a secondary detonation (e.g., Livne 1990; Woosley & Weaver 1994). These “thick-shell” models (typically  $M_{\text{He}} \gtrsim 0.1 M_{\odot}$ ) also highlighted a tension: extensive He-shell

burning at high velocity seeds outer iron-group and intermediate-mass material (notably Ti, Cr, Ca) that can produce strong line blanketing and redder colors than normal SNe Ia (Woosley & Weaver 1994). Motivated by this, the field pivoted to “thin-shell” realizations where  $M_{\text{He}} \lesssim 0.05 M_{\odot}$  suffices to trigger the core while minimizing high-velocity shell ash (Fink et al. 2010; Kromer et al. 2010; Woosley & Kasen 2011).

Our setup deliberately revisits the historical thick-shell regime, but with physically time-evolved, quiescent He envelopes as initial conditions for the explosion phase. This lets us test whether shock focusing and core ignition remain robust under modern numerics while reassessing how outer IME/IGE ash maps onto observables (radiative transfer is deferred to a follow-up paper). The hydrodynamic outcome here, a shell detonation that triggers a core detonation, is consistent with multi-D demonstrations of ignition robustness across shell masses (Livne 1990; Fink et al. 2010).

### 1.2. Relation to prior simulations

Multi-D work since the 1990s finds that once a lateral He detonation wraps the star, the inward shock can reach core-ignition conditions over broad parameters (Livne 1990; Fink et al. 2010). Where models diverge is in the *observable* imprint of the shell ash. Thin, modestly polluted shells ( $M_{\text{He}} \lesssim 0.05 M_{\odot}$ ) tend to yield bluer colors and spectra closer to normal SNe Ia (Kromer et al. 2010; Woosley & Kasen 2011), whereas thicker shells enhance Ca/Ti/Cr at high velocity and can redden the early-time SED (Woosley & Kasen 2011). Systematic grids connecting shell mass/composition to light-curve and spectral behavior (Polin et al. 2019) further indicate that the “massive-shell” regime better matches peculiar, strongly line-blanketed cases (e.g., SN 2018byg) than the bulk of normal SNe Ia.

Our fiducial model lies on the “thicker-shell” side of these mappings, but with a stratifica-

tion and small residual He mass that may mitigate the most extreme color effects (see Section 4.1.1). Here we emphasize the dynamical robustness and nucleosynthetic budgets and quantify the outer-shell IME/IGE yields against the literature ranges; detailed radiative transfer is beyond this paper’s scope.

## 2. METHODS

We begin from the quiescent helium-accretion model #23 of Hillman et al. (2025) (see there, Tables 1 and 3). A  $0.7 M_{\odot}$  carbon–oxygen (CO) white dwarf (WD) accretes helium at  $\dot{M} = 10^{-8} M_{\odot} \text{yr}^{-1}$  and grows to  $1.1 M_{\odot}$ . The one-dimensional (1D) hydrodynamic Lagrangian nova code used by Hillman et al. (2025) follows consecutive eruptions from helium accretion. Originally developed for hydrogen-rich accretion (Priainik & Kovetz 1995; Yaron et al. 2005; Epelstain et al. 2007; Hillman et al. 2015), the code was adapted for helium accretion as in Hillman et al. (2016) to quantify how much helium a WD can retain prior to a thermonuclear runaway (TNR). We extract a snapshot immediately before explosive burning (i.e., before Si-group burning becomes numerically unresolved in 1D), yielding hydrostatic radial profiles  $\{\rho(r), T(r), X_i(r)\}$  of a helium-rich envelope over a CO core as functions of enclosed mass and radius. Figure 1 summarizes the long-term envelope growth and core composition evolution for several  $(M_{\text{WD},i}, \dot{M})$  tracks from Hillman et al. (2025); our fiducial track is  $M_{\text{WD},i} = 0.7 M_{\odot}$ ,  $\dot{M} = 10^{-8} M_{\odot} \text{yr}^{-1}$ .

The explosive phase is modeled with FLASH 4.7 (Fryxell et al. 2000), solving the compressible Euler equations in three dimensions with the unsplit solver (Lee 2006; Lee & Deane 2009; Lee 2013) and self-gravity via the multipole Poisson solver. Microphysics includes the Helmholtz electron–positron Fermi–Dirac equation of state (degenerate/relativistic electrons and positrons, ideal ions with Coulomb corrections, and radiation; Aparicio (1998);

Timmes & Arnett (1999); Timmes & Swesty (2000)), and nuclear energy generation with the approximate 19-isotope  $\alpha$ -chain network (Weaver et al. 1978), which captures the dominant energy-releasing flows for helium burning and CO detonation.

Profiles are remapped from the Lagrangian grid to the FLASH Eulerian mesh using a mass-conservative interpolation that preserves zone-integrated mass, momentum, and internal energy. We then perform a brief hydrostatic relaxation with nuclear reactions disabled, self-gravity enabled, and a velocity-proportional damping term that decays exponentially over a few dynamical times. After relaxation, the model is hydrodynamically stable, and the central density and temperature remain within  $<1\%$  of their mapped values.

Adaptive mesh refinement (AMR) is applied *only* on density and temperature gradients so as to track the detonation front and the core-shell interface cleanly. The finest cell size is  $\simeq 7$  km, ensuring enough fine cells across the numerically broadened fronts in both the helium shell and the upper CO core.

To seed ignition with a minimal perturbation, we introduce an *off-axis* Gaussian temperature hotspot centered at  $(r, \theta, \phi) = (2470 \text{ km}, 60^\circ, 30^\circ)$  with characteristic radius  $\sigma_r = 200$  km and peak temperature  $T_{\text{max}} = 3 \times 10^8$  K. In the 1D Lagrangian models, the local base temperature naturally approaches this perturbed value prior to runaway; however, mapping such a temperature to an extended shell in 3D would artificially inflate the heated mass. We therefore apply the perturbation to a single point (resolved region) only in order to avoid overheating the shell while still capturing a physically plausible hotspot trigger. The resulting pre-ignition thermal and density structures are shown in Figure 2.

For nucleosynthesis diagnostics, we seed  $10^6$  Lagrangian tracer particles uniformly in a box

enclosing the WD and retain those with sufficiently high pre-detonation density to undergo significant burning, yielding a working set of  $\sim 4 \times 10^5$  tracers. For each tracer we record  $(t, \rho, T, \{X_i\})$  at the reaction substep cadence and post-process with a 127-isotope network (Paxton et al. 2015) to obtain elemental/isotopic yields and composition-versus-velocity structures.

### 3. RESULTS

We begin the explosion simulation from the relaxed mapped model. Our fiducial run yields a clear double-detonation sequence: a helium-shell detonation that sweeps laterally around the star, and an inwardly propagating shock that strengthens by geometric convergence and ignites a secondary CO detonation, unbinding the white dwarf. Figure 3 presents a zoomed time series through this sequence; the full 3D computational domain spans  $10^{11}$  cm in each direction, but for clarity we show only the central region. Columns correspond to eight epochs from  $t = 21.1$  to 393.6 ms after the temperature perturbation is applied. The top two rows show equatorial ( $x-y$ ) slices of temperature and density. Subsequent rows display, for selected species, the  $z$ -integrated mass (surface mass) distributed across the ( $x-y$ ) plane. The temperature panels capture the rapid onset and lateral wrap-around of the He detonation; the density panels show the expected rarefaction behind the front and compression within the core prior to secondary ignition. The composition panels (He, C, O, Si, Fe, Ni) trace the progression from helium combustion in the shell, through intermediate-mass element (IME) production, to iron-group element (IGE) synthesis once the core detonates. As time proceeds, He, C, and O are depleted while Si, Fe, and Ni increase. By the last column, the burning is essentially complete, and the flow is accelerating outward.

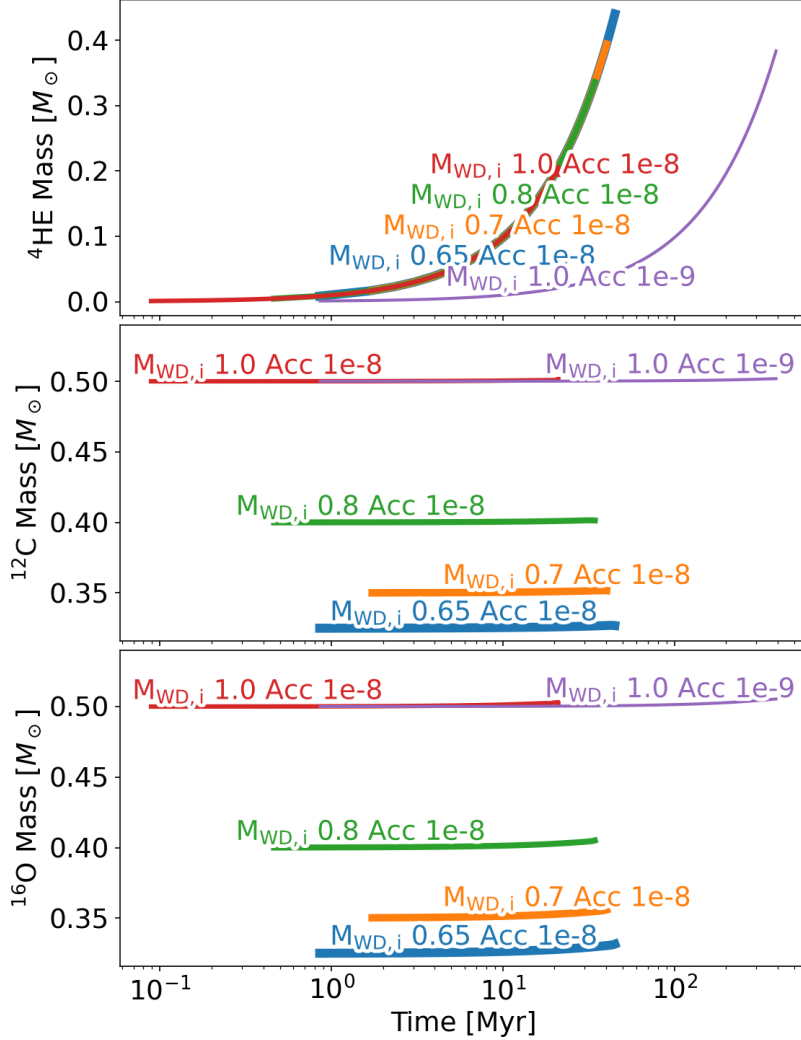


**Figure 1. Long-term envelope and core evolution in quiescent accretion models.** Helium mass (top) and bulk core carbon/oxygen masses (middle/bottom) versus time for several ( $M_{\text{WD},i}, \dot{M}$ ) tracks in Hillman et al. (2025). Our fiducial model (orange) starts at  $M_{\text{WD},i} = 0.7 M_{\odot}$  with  $\dot{M} = 10^{-8} M_{\odot} \text{ yr}^{-1}$  and grows to  $1.1 M_{\odot}$ . These models experienced uninterrupted prolonged helium accretion until indicating a SN ignition.

We follow the ejecta to  $t = 10$  s, by which time the expansion is effectively homologous. The velocity–mass relation is monotonic with maximum speeds of  $\simeq 2.2 \times 10^4 \text{ km s}^{-1}$ , consistent with normal SNe Ia. Any modest asymmetry introduced by the off–axis temperature perturbation is largely erased by the rapid wrap–around

of the shell detonation and is not expected to leave observable signatures.

Integrated elemental yields from tracer post–processing are listed in Table 1. The model synthesizes  $M(^{56}\text{Ni}) \simeq 0.64 M_{\odot}$ , indicative of a normal–luminosity SN Ia. The intermediate–mass element yield is  $M_{\text{IME}} \simeq 0.41 M_{\odot}$ ,

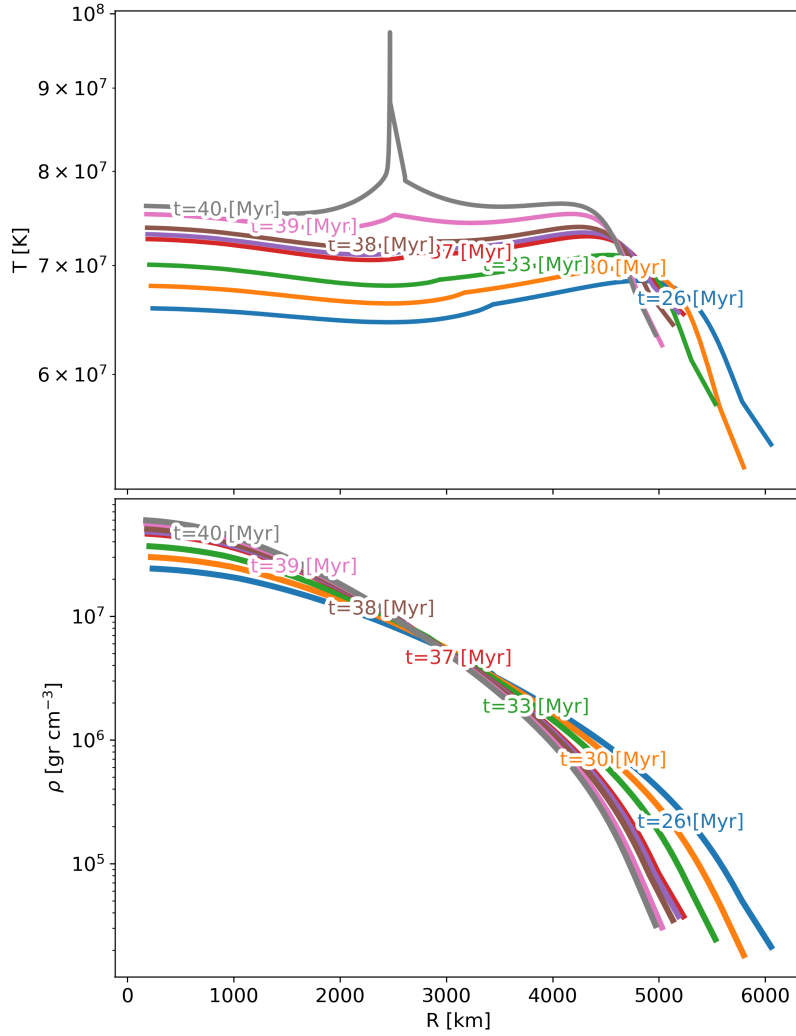


**Figure 2. Pre-ignition structure during uninterrupted helium accretion.** Temperature (top) and density (bottom) as functions of radius at several epochs in our fiducial 1D Lagrangian model. The narrow temperature spike at  $r \simeq 2.5 \times 10^3$  km marks the naturally emerging base-of-shell peak reached a few timesteps before the 1D calculation becomes numerically unresolved ( $T_{\max} \approx 3 \times 10^8$  K). In the multi-D FLASH simulations we do not map this peak to an entire shell; instead, we represent it as a localized off-axis Gaussian hotspot to avoid artificially overheating a shell while preserving the physical trigger.

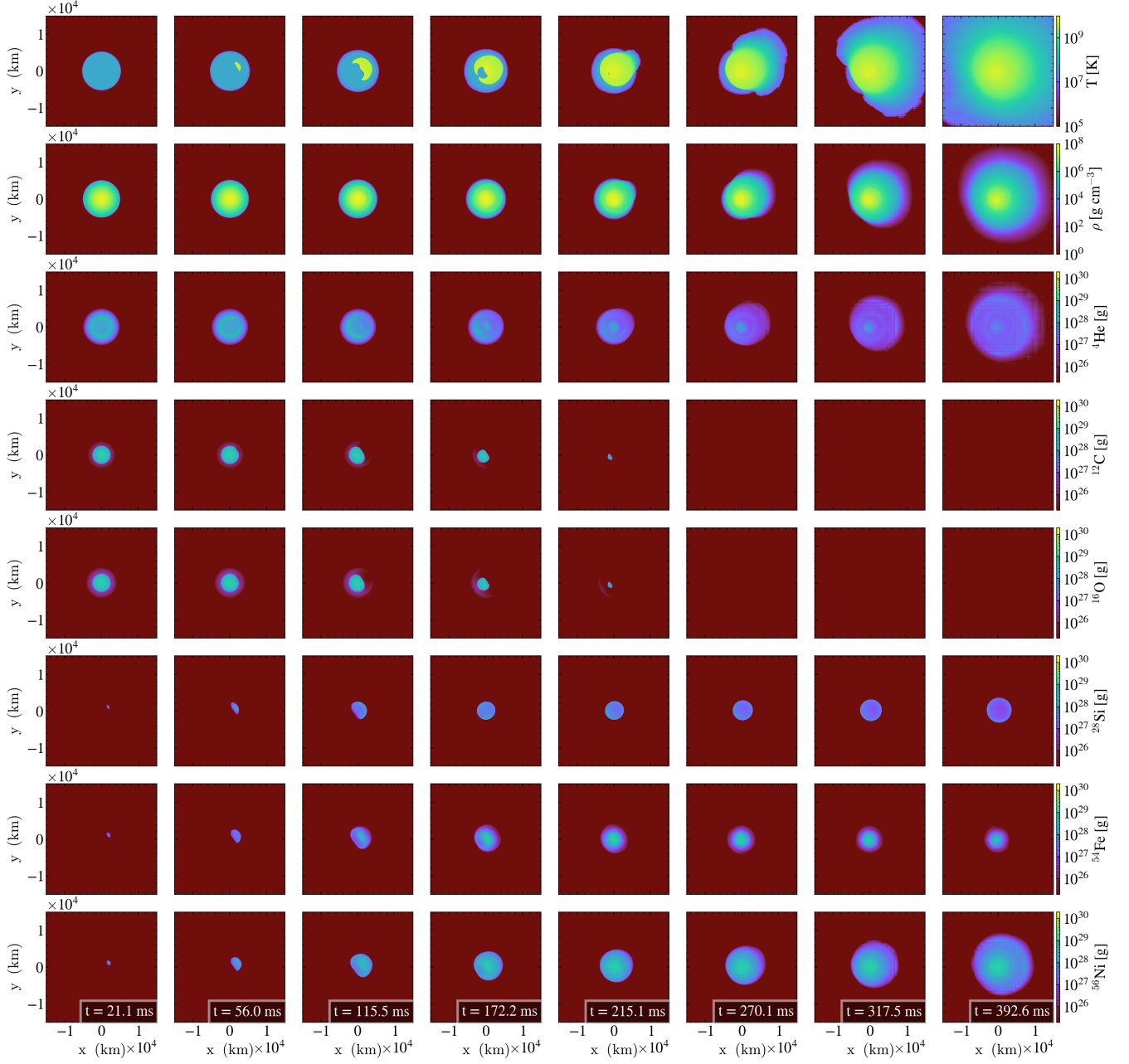


**Figure 3. Time sequence of the double detonation.** Equatorial ( $x - y$ ) slices of temperature and density (top rows), followed by  $z$ -integrated species maps (He, C, O, Si, Fe, Ni), at  $t = \{21.1, 56.0, 115.5, 172.2, 215.1, 270.1, 317.5, 392.6\}$  ms. The helium-shell detonation wraps around the star while an inward shock compresses the CO core and triggers secondary ignition. He/C/O are depleted as Si/Fe/Ni are produced. By  $\sim 0.5$  s the detonation phase is complete and the ejecta accelerate outward.

while the total iron–group mass is  $\simeq 0.66 M_{\odot}$ . While the progenitor accumulated a substantial helium envelope during its growth phase ( $\simeq 0.4 M_{\odot}$ , as shown in Figure 2), the final ejecta consists of only  $M(\text{He}) \simeq 6.7 \times 10^{-3} M_{\odot}$  unburned He. Residual CO is represented by  $M(\text{O}) \simeq 9.1 \times 10^{-4} M_{\odot}$  and  $M(\text{C}) \simeq 1.9 \times 10^{-6} M_{\odot}$ . Trace shell–ash species (e.g., Ti, Cr, Mn, V, K, Cl) are present at the  $10^{-6}$ – $10^{-2} M_{\odot}$  level.

The final abundance stratification is shown in Figure 4, which plots angle–averaged mass fractions versus the initial enclosed–mass coordinate  $M/M_{\odot}$  associated with each tracer. The inner  $\sim$ half of the ejecta are nickel–dominated (mass fraction  $\approx 1$ ), transitioning outward to an IME mantle (Si, S, Ar, Ca) and then to a thin skin of shell ashes at the highest mass coordinates. The rise of IMEs beyond  $M \approx 0.4$ – $0.5 M_{\odot}$  and enhanced Ca/Ar in the exterior are hallmarks of sub–Chandrasekhar double detonations and naturally map to line–forming regions at intermediate and high velocities.

Finally, we calculate the abundance–versus–mass structure to velocity space using the angle–averaged homologous field at the final snapshot. The nickel–dominated core occupies the lowest velocities,  $v \lesssim (7\text{--}8) \times 10^3 \text{ km s}^{-1}$ . The IME mantle (Si, S, Ar, Ca) spans intermediate velocities of order  $(8\text{--}16) \times 10^3 \text{ km s}^{-1}$ , naturally encompassing the range where strong Si II and S II features typically form. The He–shell ashes are confined to the outermost layers at  $v \gtrsim (1.6\text{--}2.2) \times 10^4 \text{ km s}^{-1}$ , consistent with the highest ejecta speeds measured in the model. These ranges vary only weakly with viewing angle (a few percent) because the shell detonation wraps around the star rapidly, leaving a largely spherical, layered structure by the time the flow becomes homologous.

#### 4. DISCUSSION

Our simulation produces a clear double detonation from a single–degenerate, helium–accumulating CO white dwarf, that built up a thick helium envelope by prolonged, quiescent accretion. The layered outcome—an inner  $^{56}\text{Ni}$ –dominated core ( $\simeq 0.64 M_{\odot}$ ), an IME mantle ( $M_{\text{IME}} \simeq 0.41 M_{\odot}$ ), and high–velocity shell ashes—together with maximum ejecta speeds of  $\sim 2.2 \times 10^4 \text{ km s}^{-1}$ , is characteristic of normal–luminosity SNe Ia from sub–Chandrasekhar explosions. In this framework, several observational facets emerge naturally.

First, the abundance layering and velocity partition suggest standard photospheric–phase line formation: Si II and S II at  $\sim (8\text{--}16) \times 10^3 \text{ km s}^{-1}$ , Ca II features (including potential high–velocity components) at the outer edge of the IME layer and into the shell ashes, and rapid color evolution governed by the  $^{56}\text{Ni}$  distribution. The small residual C/O masses ( $M(\text{C}) \sim 2 \times 10^{-6} M_{\odot}$ ;  $M(\text{O}) \sim 9 \times 10^{-4} M_{\odot}$ ) imply weak or absent early C II signatures, while the non–negligible Ca and trace Ti ( $M(\text{Ca}) \simeq 0.045 M_{\odot}$ ;  $M(\text{Ti}) \simeq 2.2 \times 10^{-4} M_{\odot}$ ) point to possible high–velocity Ca II and mild early UV/blue suppression. These tendencies align qualitatively with early–excess SNe Ia where a shallow outer  $^{56}\text{Ni}$  component or shell ashes have been invoked, yet they also highlight the degeneracy of interpretations (e.g., the diversity seen in SN 2023bee and transitional events like SN 2022xkq). A decisive test will come from radiative–transfer comparisons using our fully stratified ejecta (density+composition versus velocity) to predict early flux excesses, color evolution, and high–velocity features (HVF’s).

Independent, remnant–phase support for this layered structure has emerged from integral–field spectroscopy of the young LMC remnant SNR 0509–67.5. High–resolution MUSE data reveal a *double–shell* morphology in highly

Atom	Mass ( $M_{\odot}$ )
$^{28}\text{Ni}$	$6.4 \times 10^{-1}$
$^{27}\text{Co}$	$1.7 \times 10^{-4}$
$^{26}\text{Fe}$	$1.8 \times 10^{-2}$
$^{25}\text{Mn}$	$4.4 \times 10^{-5}$
$^{24}\text{Cr}$	$1.1 \times 10^{-2}$
$^{23}\text{V}$	$3.6 \times 10^{-6}$
$^{22}\text{Ti}$	$2.2 \times 10^{-4}$
$^{20}\text{Ca}$	$4.5 \times 10^{-2}$
$^{19}\text{K}$	$2.6 \times 10^{-6}$
$^{18}\text{Ar}$	$2.7 \times 10^{-2}$
$^{17}\text{Cl}$	$5.2 \times 10^{-6}$
$^{16}\text{S}$	$1.2 \times 10^{-1}$
$^{15}\text{P}$	$4.0 \times 10^{-5}$
$^{14}\text{Si}$	$2.2 \times 10^{-1}$
$^{12}\text{Mg}$	$1.8 \times 10^{-5}$
$^8\text{O}$	$9.1 \times 10^{-4}$
$^6\text{C}$	$1.9 \times 10^{-6}$
$^2\text{He}$	$6.7 \times 10^{-3}$

**Table 1. Elemental yields (high  $Z$  to low  $Z$ ).** Integrated ejecta masses (in  $M_{\odot}$ ) for selected species, ordered by atomic number  $Z$  from highest to lowest. Values are derived from tracer post-processing with a 127-isotope network at the epoch when the ejecta are effectively homologous. Only a representative subset is shown.

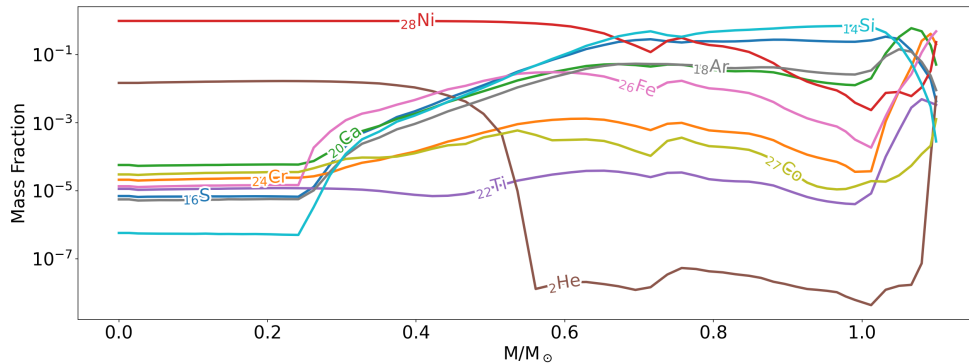


**Figure 4. Abundance stratification in mass coordinates.** Angle-averaged mass fractions binned by the tracers' initial enclosed-mass coordinate  $M/M_{\odot}$ , evaluated once the ejecta are homologous. The inner ejecta are dominated by nickel, followed by an IME mantle (Si, S, Ar, Ca), and a thin outer layer of shell ashes.

ionized calcium ([Ca XV]) and a single sulphur shell in the reverse-shocked ejecta. The outer Ca shell is naturally interpreted as the product of the helium-layer detonation, while the inner Ca shell arises from incomplete burning in the CO-core detonation—precisely the stratification expected from sub-Chandrasekhar double detonations. This “double-shell Ca” fingerprint provides spatially resolved, remnant-phase evidence that the double-detonation mechanism operates in nature (Das et al. 2025; Soker 2025b). Second, the total  $^{56}\text{Ni}$  mass is adequate for normal peak luminosities without requiring near-Chandrasekhar densities or strong electron captures. The comparatively low stable iron-peak content ( $M(\text{Fe}) \simeq 0.018 M_{\odot}$ ; trace Mn/Cr) is consistent with sub-Chandrasekhar densities at burning and should imprint itself in nebular ratios (e.g.,  $[\text{Fe III}]/[\text{Fe II}]$ ,  $[\text{Ni II}]/[\text{Fe II}]$ ) at  $\gtrsim 200$  days. Because the small off-axis temperature perturbation is rapidly overtaken by the wrapping He detonation, global asymmetries are muted at homology and are unlikely to leave observable signatures or strong continuum polarization.

Third, in the broader progenitor context, this work strengthens the case that *quiescent* single-degenerate helium accretors can reach double-detonation conditions, even at sub-Chandrasekhar masses. In the 1D evolutionary tracks we build upon, specific combinations of WD mass, core temperature, and  $\dot{M} \gtrsim 10^{-8} M_{\odot} \text{yr}^{-1}$  allow the system to avoid discrete He-nova ejections, steadily amassing a shell until runaway. Our mapped profiles thus provide physically motivated seeds for the hydrodynamic phase, as opposed to ad hoc shell prescriptions. From a demographics perspective, such systems would naturally populate intermediate delay times and evade many SD observational constraints (no H lines, faint/compact donors, low CSM signatures), complementing double-degenerate channels and

potentially helping to reconcile the observed diversity of early light curves and spectra.

Potential helium donors in the single-degenerate path include (i) compact, non-degenerate He stars (e.g., post-interaction sdB/sdO-like objects) transferring through Roche-lobe overflow; (ii) stripped subgiants with He-rich envelopes; (iii) H-nova producing systems where the average cyclic accretion rate is high enough to leave a He-rich residue that accumulates over hundreds (or thousands) of eruptions; and (iv) H-rich donors that, under steady H burning, quietly build a He layer on the WD over long intervals. Hillman et al. (2025) showed that at  $\dot{M} \approx 10^{-8} M_{\odot} \text{yr}^{-1}$  a CO WD can, under specific conditions, continue helium accumulation without triggering recurrent He novae, naturally reaching the pre-detonation structures we employ here. Observationally, such donors can be UV-bright yet optically modest; combined with the lack of strong winds, they are consistent with the non-detections of luminous companions and tight radio/X-ray limits in nearby SNe Ia. Future constraints may come from deep pre-explosion UV imaging in star-forming hosts, as well as post-explosion searches for faint survivors.

#### 4.1. Caveats

Naturally, our models hold various caveats. While our network captures the dominant energy release, detailed isotopic ratios (e.g., stable Ni and Mn/Cr) are best constrained through tracer post-processing and full radiative-transfer modeling for direct comparison with nebular spectra. Resolution and perturbation-placement indicate robustness of the outcome (He detonation followed by core ignition), but a broader parameter study—including shell mass, WD mass, and accretion history—will quantify the breadth of normal versus sub-luminous outcomes and the strength of early bumps and HVFs. Finally, connecting these models to rates requires cou-

pling binary–population synthesis for helium donors with retention efficiencies calibrated to long–term He–nova evolution. To complete the picture, the “undetermined transient” branch identified by Hillman et al. (2025) under comparable accretion conditions should also be subjected to the same multi-D explosion and radiative-transfer analysis, to determine whether it leads to faint thermonuclear transients or non-explosive outcomes.

#### 4.1.1. *IME/IGE in the outer ejecta*

A known vulnerability of thick-shell double detonations is the chemical makeup of the outer  $v \gtrsim 1.5 \times 10^4 \text{ km s}^{-1}$  layers. He detonations at  $\rho \sim 10^5\text{--}10^6 \text{ g cm}^{-3}$  can synthesize significant Ca and, depending on pollution, Ti/Cr, while leaving some residual He (Woosley & Weaver 1994; Shen & Moore 2014). These species shape early UV/blue opacity and can drive prominent high-velocity Ca II features. Grids and case studies indicate that more massive shell or shells with low C/N pollution tend to produce stronger UV suppression and redder  $g - r$  at early times, with SN 2018byg providing an extreme instance (Polin et al. 2019; De et al. 2019).

To make these risks explicit, we tabulate (i)  $M(\text{Ca})$ ,  $M(\text{Ti})$ ,  $M(\text{Cr})$  above  $1.5 \times 10^4 \text{ km s}^{-1}$ , (ii) the residual He mass in the same velocity layer, and (iii) the angle-averaged velocity distributions of these species (Table 1 and Fig. 4). While radiative transfer is deferred, these numbers can be read against published thresholds for strong line blanketing and HVFs. We also note that modest shell pollution by C/O or  $^{14}\text{N}$  reduces Ti/Cr yields and can lower He I detectability by altering ionization/excitation conditions (Boyle et al. 2017; Jiang et al. 2017; Magee et al. 2022).

## 5. CONCLUSIONS AND SUMMARY

We have modeled a single–degenerate, sub–Chandrasekhar double detonation by mapping time–evolved helium–accretion profiles

into multi–D hydrodynamics and following the ejecta to homology. Our main conclusions are:

(1) *Clear double–detonation sequence.* A laterally propagating helium–shell detonation launches an inward shock that converges and ignites the CO core, unbinding the star. Burning is essentially complete by  $\sim 0.5 \text{ s}$ , and by  $t = 10 \text{ s}$  the flow is homologous.

(2) *Yields consistent with normal SNe Ia.* The explosion synthesizes  $M(^{56}\text{Ni}) \simeq 0.64 M_{\odot}$  and  $M_{\text{IME}} \simeq 0.41 M_{\odot}$ , with a total iron–group mass of  $\simeq 0.66 M_{\odot}$ . Residual unburned masses are small ( $M(\text{He}) \simeq 6.7 \times 10^{-3} M_{\odot}$ ,  $M(\text{O}) \simeq 9.1 \times 10^{-4} M_{\odot}$ ,  $M(\text{C}) \simeq 1.9 \times 10^{-6} M_{\odot}$ ), and maximum ejecta speeds reach  $\simeq 2.2 \times 10^4 \text{ km s}^{-1}$ .

(3) *Layered ejecta and kinematic partition.* The nickel–dominated core occupies the lowest velocities, an IME mantle (Si, S, Ar, Ca) spans  $(8\text{--}16) \times 10^3 \text{ km s}^{-1}$ , and He–shell ashes reside at  $\gtrsim (1.6\text{--}2.2) \times 10^4 \text{ km s}^{-1}$ . The rapid wrap–around of the shell detonation erases most large–scale asymmetries, so strong viewing–angle effects are not expected.

(4) *Early–time spectral tendencies.* The enhanced Ca and trace Ti in the outer layers imply strong Ca II H&K (and possible HVFs) and mild UV/blue suppression from line blanketing at early times, fading as the photosphere recedes beneath the shell–ash layer. These signatures, together with the stratified IME/IGE structure, provide testable predictions for light curves and spectra.

(5) *Progenitor implications.* Prolonged, quiescent helium accretion at  $\dot{M} \lesssim 10^{-8} M_{\odot} \text{ yr}^{-1}$  can build the pre–detonation shells required for double detonations, consistent with compact He–star donors or He–rich channels discussed in prior evolutionary work. Such systems naturally avoid many classic SD constraints (no H lines, weak CSM) while contributing to the diversity of early–time behaviors.

Beyond these findings, our model aligns qualitatively with remnant–phase evidence for lay-

ered double detonations (e.g., a double-shell calcium morphology), encouraging targeted radiative-transfer comparisons. Immediate next steps include (i) synthetic light curves and spectra from the stratified ejecta for direct confrontation with high-cadence data; (ii) a parameter survey in WD mass, shell mass, and accretion history to chart  $^{56}\text{Ni}$  and IME yields, early bumps, and HVFs; and (iii) coupling to binary-population synthesis for helium donors, with retention efficiencies informed by long-baseline helium-nova evolution, to assess rates and delay-time distributions. Together,

these efforts will clarify how frequently *quiescent* helium accretors produce normal SNe Ia and what observational features most clearly distinguish this channel.

## ACKNOWLEDGMENTS

We acknowledge support for this project from the European Union’s Horizon 2020 research and innovation program under grant agreement No 865932-ERC-SNeX. This work was supported by the Azrieli College of Engineering – Jerusalem Research Fund.

## REFERENCES

- Abate, C., Pols, O. R., Izzard, R. G., Mohamed, S. S., & de Mink, S. E. 2013, *A&A*, 552, A26, doi: [10.1051/0004-6361/201220007](https://doi.org/10.1051/0004-6361/201220007)
- Aparicio, J. M. 1998, *ApJS*, 117, 627, doi: [10.1086/313121](https://doi.org/10.1086/313121)
- Bhattacharya, S., Arnaboldi, M., Gerhard, O., Kobayashi, C., & Saha, K. 2025, *ApJL*, 983, L30, doi: [10.3847/2041-8213/adc735](https://doi.org/10.3847/2041-8213/adc735)
- Boos, S. J., Townsley, D. M., & Shen, K. J. 2024, *ApJ*, 972, 200, doi: [10.3847/1538-4357/ad5da2](https://doi.org/10.3847/1538-4357/ad5da2)
- Boyle, A., Sim, S. A., Hachinger, S., & Kerzendorf, W. 2017, *A&A*, 599, A46, doi: [10.1051/0004-6361/201629712](https://doi.org/10.1051/0004-6361/201629712)
- Brout, D., Scolnic, D., Kessler, R., et al. 2019, *ApJ*, 874, 150, doi: [10.3847/1538-4357/ab08a0](https://doi.org/10.3847/1538-4357/ab08a0)
- Calder, A. C., Plewa, T., Vladimirova, N., Lamb, D. Q., & Truran, J. W. 2004, arXiv e-prints, astro, doi: [10.48550/arXiv.astro-ph/0405162](https://doi.org/10.48550/arXiv.astro-ph/0405162)
- Cavichia, O., Mollá, M., Bazán, J. J., et al. 2024, *MNRAS*, 532, 2331, doi: [10.1093/mnras/stae1626](https://doi.org/10.1093/mnras/stae1626)
- Das, P., Seitzzahl, I. R., Ruiter, A. J., et al. 2025, *Nature Astronomy*, doi: [10.1038/s41550-025-02589-5](https://doi.org/10.1038/s41550-025-02589-5)
- De, K., Kasliwal, M. M., Polin, A., et al. 2019, *ApJL*, 873, L18, doi: [10.3847/2041-8213/ab0aec](https://doi.org/10.3847/2041-8213/ab0aec)
- De, S., Timmes, F. X., Brown, E. F., et al. 2014, *ApJ*, 787, 149, doi: [10.1088/0004-637X/787/2/149](https://doi.org/10.1088/0004-637X/787/2/149)
- Epelstain, N., Yaron, O., Kovetz, A., & Prialnik, D. 2007, *MNRAS*, 374, 1449
- Fink, M., Röpke, F. K., Hillebrandt, W., et al. 2010, *A&A*, 514, A53, doi: [10.1051/0004-6361/200913892](https://doi.org/10.1051/0004-6361/200913892)
- Freundlich, J., & Maoz, D. 2021, *MNRAS*, 502, 5882, doi: [10.1093/mnras/stab493](https://doi.org/10.1093/mnras/stab493)
- Friedmann, M., & Maoz, D. 2018, *MNRAS*, 479, 3563, doi: [10.1093/mnras/sty1664](https://doi.org/10.1093/mnras/sty1664)
- Fryxell, B., Olson, K., Ricker, P., et al. 2000, *ApJS*, 131, 273, doi: [10.1086/317361](https://doi.org/10.1086/317361)
- Galbany, L., de Jaeger, T., Riess, A. G., et al. 2023, *A&A*, 679, A95, doi: [10.1051/0004-6361/202244893](https://doi.org/10.1051/0004-6361/202244893)
- Gallagher, J. S., & Starrfield, S. 1978, *ARA&A*, 16, 171, doi: [10.1146/annurev.aa.16.090178.001131](https://doi.org/10.1146/annurev.aa.16.090178.001131)
- Gamezo, V. N., Khokhlov, A. M., & Oran, E. S. 2004, *PhRvL*, 92, 211102, doi: [10.1103/PhysRevLett.92.211102](https://doi.org/10.1103/PhysRevLett.92.211102)
- . 2005, *ApJ*, 623, 337, doi: [10.1086/428767](https://doi.org/10.1086/428767)
- Glanz, H., Perets, H. B., & Pakmor, R. 2025, *ApJ*, 988, 184, doi: [10.3847/1538-4357/ade146](https://doi.org/10.3847/1538-4357/ade146)
- Hachisu, I., & Kato, M. 2010, *ApJ*, 709, 680
- Hillman, Y., & Kashi, A. 2021, *MNRAS*, 501, 201, doi: [10.1093/mnras/staa3600](https://doi.org/10.1093/mnras/staa3600)
- Hillman, Y., Michaelis, A., & Perets, H. B. 2025, arXiv e-prints, arXiv:2503.12586, doi: [10.48550/arXiv.2503.12586](https://doi.org/10.48550/arXiv.2503.12586)
- Hillman, Y., Prialnik, D., Kovetz, A., & Shara, M. M. 2015, *MNRAS*, 446, 1924
- . 2016, *ApJ*, 819, 168, doi: [10.3847/0004-637X/819/2/168](https://doi.org/10.3847/0004-637X/819/2/168)

- Hoeflich, P. 2017, in Handbook of Supernovae, ed. A. W. Alsabti & P. Murdin, 1151, doi: [10.1007/978-3-319-21846-5\\_56](https://doi.org/10.1007/978-3-319-21846-5_56)
- Howell, D. A. 2011, Nature Communications, 2, 350, doi: [10.1038/ncomms1344](https://doi.org/10.1038/ncomms1344)
- Iben, Jr., I., & Tutukov, A. V. 1984, ApJS, 54, 335, doi: [10.1086/190932](https://doi.org/10.1086/190932)
- Idan, I., Shaviv, N. J., & Shaviv, G. 2013, MNRAS, 433, 2884
- Jha, S. W., Maguire, K., & Sullivan, M. 2019, Nature Astronomy, 3, 706, doi: [10.1038/s41550-019-0858-0](https://doi.org/10.1038/s41550-019-0858-0)
- Jiang, J.-A., Doi, M., Maeda, K., et al. 2017, Nature, 550, 80, doi: [10.1038/nature23908](https://doi.org/10.1038/nature23908)
- Jordan, IV, G. C., Fisher, R. T., Townsley, D. M., et al. 2008, ApJ, 681, 1448, doi: [10.1086/588269](https://doi.org/10.1086/588269)
- Jordan, IV, G. C., Graziani, C., Fisher, R. T., et al. 2012, ApJ, 759, 53, doi: [10.1088/0004-637X/759/1/53](https://doi.org/10.1088/0004-637X/759/1/53)
- José, J., Hernanz, M., & Isern, J. 1993, A&A, 269, 291
- Kato, M., & Hachisu, I. 1999, ApJLetters, 513, L41
- . 2004, ApJLetters, 613, L129
- Khokhlov, A. M. 1991, A&A, 245, 114
- Kromer, M., Sim, S. A., Fink, M., et al. 2010, ApJ, 719, 1067, doi: [10.1088/0004-637X/719/2/1067](https://doi.org/10.1088/0004-637X/719/2/1067)
- Kushnir, D., Katz, B., Dong, S., Livne, E., & Fernández, R. 2013, ApJL, 778, L37, doi: [10.1088/2041-8205/778/2/L37](https://doi.org/10.1088/2041-8205/778/2/L37)
- Lee, D. 2006, PhD thesis, University of Maryland, College Park
- . 2013, Journal of Computational Physics, 243, 269, doi: [10.1016/j.jcp.2013.02.049](https://doi.org/10.1016/j.jcp.2013.02.049)
- Lee, D., & Deane, A. E. 2009, Journal of Computational Physics, 228, 952, doi: [10.1016/j.jcp.2008.08.026](https://doi.org/10.1016/j.jcp.2008.08.026)
- Li, W., Bloom, J. S., Podsiadlowski, P., et al. 2011, Nature, 480, 348, doi: [10.1038/nature10646](https://doi.org/10.1038/nature10646)
- Liu, D., Wang, B., Wu, C., & Han, Z. 2017, A&A, 606, A136, doi: [10.1051/0004-6361/201629788](https://doi.org/10.1051/0004-6361/201629788)
- Liu, Z.-W., Röpke, F. K., & Han, Z. 2023, Research in Astronomy and Astrophysics, 23, 082001, doi: [10.1088/1674-4527/acd89e](https://doi.org/10.1088/1674-4527/acd89e)
- Livne, E. 1990, ApJL, 354, L53, doi: [10.1086/185721](https://doi.org/10.1086/185721)
- Magee, M. R., Gillanders, J. H., Maguire, K., Sim, S. A., & Callan, F. P. 2022, MNRAS, 509, 3580, doi: [10.1093/mnras/stab3123](https://doi.org/10.1093/mnras/stab3123)
- Maoz, D., Mannucci, F., & Nelemans, G. 2014, ARA&A, 52, 107, doi: [10.1146/annurev-astro-082812-141031](https://doi.org/10.1146/annurev-astro-082812-141031)
- Meakin, C. A., Seitzzahl, I., Townsley, D., et al. 2009, ApJ, 693, 1188, doi: [10.1088/0004-637X/693/2/1188](https://doi.org/10.1088/0004-637X/693/2/1188)
- Mikolajewska, J. 2008, in Astronomical Society of the Pacific Conference Series, Vol. 401, RS Ophiuchi (2006) and the Recurrent Nova Phenomenon, ed. A. Evans, M. F. Bode, T. J. O'Brien, & M. J. Darnley, 42, doi: [10.48550/arXiv.0803.3685](https://doi.org/10.48550/arXiv.0803.3685)
- Mikolajewska, J. 2010, arXiv e-prints, doi: [10.48550/arXiv.1011.5657](https://doi.org/10.48550/arXiv.1011.5657)
- Mikolajewska, J., & Kenyon, S. J. 1992, MNRAS, 256, 177, doi: [10.1093/mnras/256.2.177](https://doi.org/10.1093/mnras/256.2.177)
- Nelemans, G., Yungelson, L. R., Portegies Zwart, S. F., & Verbunt, F. 2001, A&A, 365, 491, doi: [10.1051/0004-6361:20000147](https://doi.org/10.1051/0004-6361:20000147)
- Newsham, G., Starrfield, S., & Timmes, F. X. 2014, in Stella Novae: Past and Future Decades, ed. P. A. Woudt & V. A. R. M. Ribeiro, Vol. 490 (Astronomical Society of the Pacific Conference Series), 287–294. <https://arxiv.org/abs/1303.3642>
- Nomoto, K. 1982a, ApJ, 253, 798, doi: [10.1086/159682](https://doi.org/10.1086/159682)
- . 1982b, ApJ, 257, 780, doi: [10.1086/160031](https://doi.org/10.1086/160031)
- Nugent, P. E., Sullivan, M., Cenko, S. B., et al. 2011, Nature, 480, 344, doi: [10.1038/nature10644](https://doi.org/10.1038/nature10644)
- Pakmor, R., Kromer, M., Taubenberger, S., & Springel, V. 2013, ApJL, 770, L8, doi: [10.1088/2041-8205/770/1/L8](https://doi.org/10.1088/2041-8205/770/1/L8)
- Pakmor, R., Zenati, Y., Perets, H. B., & Toonen, S. 2021, MNRAS, 503, 4734, doi: [10.1093/mnras/stab686](https://doi.org/10.1093/mnras/stab686)
- Pakmor, R., Callan, F. P., Collins, C. E., et al. 2022, MNRAS, 517, 5260, doi: [10.1093/mnras/stac3107](https://doi.org/10.1093/mnras/stac3107)
- Palicio, P. A., Matteucci, F., Della Valle, M., & Spitoni, E. 2024, A&A, 689, A203, doi: [10.1051/0004-6361/202449740](https://doi.org/10.1051/0004-6361/202449740)
- Paxton, B., Marchant, P., Schwab, J., et al. 2015, ApJS, 220, 15, doi: [10.1088/0067-0049/220/1/15](https://doi.org/10.1088/0067-0049/220/1/15)

- Pearson, J., Sand, D. J., Lundqvist, P., et al. 2024, *ApJ*, 960, 29, doi: [10.3847/1538-4357/ad0153](https://doi.org/10.3847/1538-4357/ad0153)
- Perets, H. B., Zenati, Y., Toonen, S., & Bobrick, A. 2019, arXiv e-prints, arXiv:1910.07532, doi: [10.48550/arXiv.1910.07532](https://doi.org/10.48550/arXiv.1910.07532)
- Piro, A. L., & Nakar, E. 2025, arXiv e-prints, arXiv:2507.14290, doi: [10.48550/arXiv.2507.14290](https://doi.org/10.48550/arXiv.2507.14290)
- Plewa, T., Calder, A. C., & Lamb, D. Q. 2004, *ApJL*, 612, L37, doi: [10.1086/424036](https://doi.org/10.1086/424036)
- Polin, A., Nugent, P., & Kasen, D. 2019, *ApJ*, 873, 84, doi: [10.3847/1538-4357/aafb6a](https://doi.org/10.3847/1538-4357/aafb6a)
- Pollin, J. M., Sim, S. A., Shingles, L. J., et al. 2025, arXiv e-prints, arXiv:2507.05000, doi: [10.48550/arXiv.2507.05000](https://doi.org/10.48550/arXiv.2507.05000)
- Prialnik, D., & Kovetz, A. 1995, *ApJ*, 445, 789, doi: [10.1086/175741](https://doi.org/10.1086/175741)
- Raskin, C., Timmes, F. X., Scannapieco, E., Diehl, S., & Fryer, C. 2009, *MNRAS*, 399, L156, doi: [10.1111/j.1745-3933.2009.00743.x](https://doi.org/10.1111/j.1745-3933.2009.00743.x)
- Ruiter, A. J., & Seitzzahl, I. R. 2025, *A&A Rv*, 33, 1, doi: [10.1007/s00159-024-00158-9](https://doi.org/10.1007/s00159-024-00158-9)
- Saio, H., & Nomoto, K. 1998, *ApJ*, 500, 388, doi: [10.1086/305696](https://doi.org/10.1086/305696)
- Saladino, M. I., Pols, O. R., & Abate, C. 2019, *A&A*, 626, A68, doi: [10.1051/0004-6361/201834598](https://doi.org/10.1051/0004-6361/201834598)
- Shara, M. M. 1981, *ApJ*, 243, 926
- Shara, M. M., Prialnik, D., Hillman, Y., & Kovetz, A. 2018, *ApJ*, 860, 110
- Shen, K. J., Bildsten, L., Kasen, D., & Quataert, E. 2012, *ApJ*, 748, 35, doi: [10.1088/0004-637X/748/1/35](https://doi.org/10.1088/0004-637X/748/1/35)
- Shen, K. J., Kasen, D., Weinberg, N. N., Bildsten, L., & Scannapieco, E. 2010, *ApJ*, 715, 767, doi: [10.1088/0004-637X/715/2/767](https://doi.org/10.1088/0004-637X/715/2/767)
- Shen, K. J., & Moore, K. 2014, *ApJ*, 797, 46, doi: [10.1088/0004-637X/797/1/46](https://doi.org/10.1088/0004-637X/797/1/46)
- Soker, N. 2024, *The Open Journal of Astrophysics*, 7, 31, doi: [10.33232/001c.117147](https://doi.org/10.33232/001c.117147)
- . 2025a, arXiv e-prints, arXiv:2507.16757, doi: [10.48550/arXiv.2507.16757](https://doi.org/10.48550/arXiv.2507.16757)
- . 2025b, *The Open Journal of Astrophysics*, 8, 36, doi: [10.33232/001c.134113](https://doi.org/10.33232/001c.134113)
- Starrfield, S., & Sparks, W. M. 1987, *Ap&SS*, 131, 379, doi: [10.1007/BF00668117](https://doi.org/10.1007/BF00668117)
- Tang, S., & Wang, Q. D. 2010, *MNRAS*, 408, 1011, doi: [10.1111/j.1365-2966.2010.17171.x](https://doi.org/10.1111/j.1365-2966.2010.17171.x)
- Timmes, F. X., & Arnett, D. 1999, *ApJS*, 125, 277, doi: [10.1086/313271](https://doi.org/10.1086/313271)
- Timmes, F. X., & Swesty, F. D. 2000, *ApJS*, 126, 501, doi: [10.1086/313304](https://doi.org/10.1086/313304)
- Toonen, S., Hollands, M., Gänsicke, B. T., & Boekholt, T. 2017, *A&A*, 602, A16, doi: [10.1051/0004-6361/201629978](https://doi.org/10.1051/0004-6361/201629978)
- Vathachira, I. B., Hillman, Y., & Kashi, A. 2024, *MNRAS*, 527, 4806, doi: [10.1093/mnras/stad3507](https://doi.org/10.1093/mnras/stad3507)
- . 2025a, *ApJ*
- . 2025b, *ApJ*, 980, 224, doi: [10.3847/1538-4357/adabca](https://doi.org/10.3847/1538-4357/adabca)
- Wang, Q., Rest, A., Dimitriadis, G., et al. 2024, *ApJ*, 962, 17, doi: [10.3847/1538-4357/ad0edb](https://doi.org/10.3847/1538-4357/ad0edb)
- Warner, B. 1995, *Cambridge Astrophysics Series*, 28
- Weaver, T. A., Zimmerman, G. B., & Woosley, S. E. 1978, *ApJ*, 225, 1021, doi: [10.1086/156569](https://doi.org/10.1086/156569)
- Webbink, R. F. 1984, *ApJ*, 277, 355, doi: [10.1086/161701](https://doi.org/10.1086/161701)
- Whelan, J., & Iben, Jr., I. 1973, *ApJ*, 186, 1007, doi: [10.1086/152565](https://doi.org/10.1086/152565)
- Woosley, S. E., & Kasen, D. 2011, *ApJ*, 734, 38, doi: [10.1088/0004-637X/734/1/38](https://doi.org/10.1088/0004-637X/734/1/38)
- Woosley, S. E., & Weaver, T. A. 1994, *ApJ*, 423, 371, doi: [10.1086/173813](https://doi.org/10.1086/173813)
- Yao, Y., Miller, A. A., Kulkarni, S. R., et al. 2019, *ApJ*, 886, 152, doi: [10.3847/1538-4357/ab4cf5](https://doi.org/10.3847/1538-4357/ab4cf5)
- Yaron, O., Prialnik, D., Shara, M. M., & Kovetz, A. 2005, *ApJ*, 623, 398, doi: [10.1086/428435](https://doi.org/10.1086/428435)